Synthesis and characterisation of spherical core–shell Ag/ZnO nanocomposites using single and two – steps ultrasonic spray pyrolysis (USP)

Article *in* Catalysis Today · December 2017

DOI: 10.1016/j.cattod.2017.11.029

CITATIONS
19

READS
328

5 authors, including:

L. Muñoz
University Carlos III de Madrid
6 PUBLICATIONS **87** CITATIONS
SEE PROFILE

Gözde Alkan
German Aerospace Center (DLR)
37 PUBLICATIONS **272** CITATIONS
SEE PROFILE

Olivera Milosevic
Serbian Academy of Sciences and Arts
130 PUBLICATIONS **1,555** CITATIONS
SEE PROFILE

Maria Eugenia Rabanal
University Carlos III de Madrid
112 PUBLICATIONS **1,179** CITATIONS
SEE PROFILE

Catalysis Today xxx (xxxx) xxx–xxx

Contents lists available at ScienceDirect

Catalysis Today

journal homepage: www.elsevier.com/locate/cattod

Synthesis and characterisation of spherical core-shell Ag/ZnO nanocomposites using single and two – steps ultrasonic spray pyrolysis (USP)

L. Muñoz-Fernandez[a,*], G. Alkan[b], O. Milošević[c], M.E. Rabanal[a], B. Friedrich[b]

[a] Carlos III University of Madrid and IAAB, Department of Materials Science and Engineering and Chemical Engineering, Avda. de la Universidad 30, 28911 Leganes, Madrid, Spain[1]

[b] IME Process Metallurgy and Metal Recycling, Intzestraße 3, 52072 Aachen, Germany

[c] Institute of Technical Sciences of the Serbian Academy of Sciences and Arts, Knez Mihailova 35/IV, 11000 Belgrade, Serbia

ARTICLE INFO

Keywords:
Ag/ZnO
Core-shell structure
Ultrasonic spray pyrolysis method

ABSTRACT

Spherical core-shell Ag/ZnO nanocomposites were synthesised by ultrasonic spray pyrolysis (USP) method from zinc nitrate hexahydrate, $Zn(NO_3)_2{\cdot}6H_2O$ (ZN) and silver nitrate, $AgNO_3$ (SN) precursors. Varying solution concentrations and equipment installations (either single − or two-step USP) allowing simultaneous and consecutive precipitation of Ag and ZnO were examined regarding their effect on final particle microstructure and photocatalytic properties. Morphological analyses revealed pure Ag/ZnO core-shell structure where ZnO secondary submicron sized particles formed by primary crystals with the size of 5–20 nm. Depending on the solution concentrations and USP installations, various distributions of Ag in the final microstructure was revealed. Photocatalytic analyses (all samples reached > 45% MB degradation) confirm the all Ag/ZnO USP systems viability for environmental applications. The best result (93% of methylene blue (MB) elimination) is obtained for the sample with the maximum available surface, which strongly depends on particle morphology, size, and dispersion. Moreover, all samples synthesised by single step co-precipitation revealed higher dye elimination concerning ones with two steps precipitation due to the favoured distribution of silver nanoparticles in their microstructure and higher specific surface area. Moreover, samples with a uniform and homogeneous Ag distribution exhibited silver-induced enhancement of photocatalytic performance.

1. Introduction

Size dependent electronic and optical properties of nanostructured metals and semiconductors favour their utilisation as catalysts for the light induced chemical reactions. Especially, complex nanostructures (e.g. core-shell composite) with multicomponent are the focus of considerable interest because of their coupling properties [1–3]. Among various metal oxides, zinc oxide (ZnO) has superior performance owing to its physical and chemical stability, suitable band gap value of 3.37 eV and high catalytic activity. Moreover, when it is used in combination with a noble metal such as silver (Ag), these advantages are conserved, and some drawbacks such as low phonon energy, high photo generated electron-hole pair (e^-/h^+) recombination potential are avoided. Therefore, the photocatalytic efficiency is enhanced, and new synergetic properties are achieved originated from Ag/ZnO interface [4,5].

There have been many previous studies performed to synthesise Ag/ZnO improving their photocatalytic properties [6–9]. Zhang et al. [10] synthesised Ag/ZnO composites *via* hydrothermal method with various silver contents and reported that 1.3 mol% silver addition yields in the highest photocatalytic performance with an increase of 6.2%. Parallel findings were reported by Wang et al. [11] on Ag effect on the photocatalytic behaviour of Ag/ZnO synthesised by photo reduction method. Similarly, for the maximum performance, an optimum Ag amount of 12% was presented. After that amount, with increasing Ag concentration, they have a tendency to agglomerate which is detrimental to photocatalytic activity (PCA). It is known that when Ag nanoparticles are on the surface of the ZnO, they inhibit the recombination of photoexcited electrons and holes most effectively. However, in our previous studies [12], with one step aerosol synthesis, there has been an enormous amount of shell material detected as entrapped in core volume

* Corresponding author.
E-mail addresses: limunozf@ing.uc3m.es, lidia.munoz.fdez@gmail.com (L. Muñoz-Fernandez), galkan@metallurgie.rwth-aachen.de (G. Alkan), olivera.milosevic@itn.sanu.ac.rs (O. Milošević), mariaeugenia.rabanal@uc3m.es (M.E. Rabanal), bfriedrich@metallurgie.rwth-aachen.de (B. Friedrich).
[1] http://isni.org/0000000121689183.

https://doi.org/10.1016/j.cattod.2017.11.029
Received 3 July 2017; Received in revised form 27 October 2017; Accepted 27 November 2017

without reaching the surface, which is detrimental to PCA. To promote the silver diffusion onto ZnO surface without precipitation in volume, precursor solution concentration is the key parameter needed to be controlled. It should be adjusted in a way that first ZnO precursor reaches to critical saturation point and precipitate, while diffusion of Ag onto surface continues. Finally, precipitation of Ag on the already existing ZnO surfaces takes place. Another way to ensure phase separation and silver deposition on the surface of ZnO is the utilisation of a new installation of USP, where ZnO and Ag precipitate consecutively and/or separately. This two-step installation provides separate atomization of both precursors, where initially formed ZnO particles meet with $AgNO_3$ droplets in the second part of the reaction zone. In the case of a successful collision, silver nitrate droplets locate on the ZnO surface and decompose into metallic silver, which ensures the presence of metallic silver on ZnO surface. When compared with one step, where some Ag may be entrapped in the core volume, by two steps equipment, a superior distribution of Ag on ZnO surface may be achieved which is very promising for photocatalytic properties. Therefore; in this study, to obtain highly catalytic Ag/ZnO nanocomposites with a favoured distribution of Ag on ZnO surface, varying silver and ZnO concentrations were used for the synthesis with two modified versions of USP which enables simultaneous and consecutive precipitation of Ag and ZnO constituents, respectively. Different formation mechanisms of two USP variations and relative amounts of Ag and ZnO in products were related with the final microstructure regarding particle size, morphology and silver distribution. Moreover, photocatalytic activities of samples were examined, and the differences explained by observed microstructural variations. Most promising composition and USP synthesis conditions were proposed for highly photocatalytic Ag/ZnO systems.

2. Experimental section

2.1. Synthesis

Ag/ZnO structures with varying silver and zinc concentration were synthesised *via* ultrasonic spray pyrolysis (USP). All the chemicals used in this study were in analytical grade and used as purchased (Sigma Aldrich) without further purification. Silver nitrate ($AgNO_3$, purity > 98%) and zinc nitrate hexahydrate ($Zn(NO_3)_2{\cdot}6H_2O$, purity > 99%) were utilised as silver and zinc sources, respectively. In a typical synthesis, the precursor solutions were prepared by dissolving relative amounts of $AgNO_3$ and $Zn(NO_3)_2{\cdot}6H_2O$ in deionised water. At IME-RWTH, there are two different constructions of horizontal USP available which enable simultaneous and consecutive precipitation of two constituents, respectively. The former (a single step USP) can be considered as standard USP with main parts of ultrasound generator (Gapusol, RBI, France), a carrier gas inlet connected to a flow regulator, horizontal wall heated furnace with a quartz tube and washing bottles for collection purposes. Details of this experimental setup can be found elsewhere [13]. The latter equipment (two-step USP) is schematically shown in Fig. S1. Two ultrasound generators were utilised where zinc nitrate and silver nitrate solutions were separately atomised. Moreover, the quartz reaction tube in furnaces exhibits different size (diameter, length) and a specific T geometry functioning as a connection zone. Zn $(NO_3)_2$ droplets formed by the first generator (2.5 MHz) were transferred to the first part of tubular quartz reactor at 800 °C with a flow rate of 1.5 ml/min nitrogen, as carrier gas, to experience thermal decomposition to ZnO. Between two heating zones at the T-connection part, the gas carrying ZnO product of the first zone was mixed with the stream consisting $AgNO_3$ droplets produced by the second generator (2.5 MHz) and they were transferred to the second heating zone together, where the decomposition of $AgNO_3$ to Ag takes place. Reaction products were collected in washing bottles filled with ethanol and subsequently dried in an air atmosphere at 90 °C until the complete solvent evaporates. Based on a previous study, the optimal gas volume flow and reaction temperature were selected [12]. Two different concentrations (high (H) and low (L)) of zinc (Z) and silver (S) have been used for the Ag/ZnO synthesis via one (1) and two (2) steps USP. Details of synthesis conditions and sample abbreviations can be found in Table S1.

2.2. Characterization

XRD patterns were recorded in the range between 2θ = 10°–90°, at room temperature (RT) with a Philips X'Pert X-ray diffractometer with Cu K_α radiation ($\lambda_{\alpha 1} \approx 1.5406$ Å) for carrying out the structural characterisation. The average crystallite size (CS) can be estimated using Scherrer formula, $D = 0.9\,\lambda_{\alpha 1}/(\beta_D \cos\theta)$, where D is the crystallite size (in Å), $\lambda_{\alpha 1}$ is the wavelength of the X-ray diffraction (in Å), β_D is the FWHM (full width at half maximum, corrected for instrumental broadening) and θ is the peak position (in °) [5].

Surface morphology, chemical composition and particle sizes were studied by a Philips XL 30/EDAX-Dx4 Scanning Electron Microscope (SEM) and a JEOL JEM 2100 Transmission Electron Microscope (TEM). By micrograph analyses, secondary particle sizes were measured and averaged by several particles (n = 20). The optical properties were determined by diffuse reflectance spectroscopy (DRS) using a 60 mm integrator sphere and $BaSO_4$ as a pattern on a Lambda 14P, Perkin-Elmer UV–vis spectrophotometer. Band gap values were experimentally determined through Kubelka–Munk formula: $F(R) = (1-R_\infty)^2/2R_\infty$ [13,14], where R_∞ is the reflectance of samples. The N_2 adsorption/desorption was carried out in a Micromeritics Gemini VII instrument (at 196.6 °C). Before experiments, the samples were outgassed at 90 °C overnight. The specific surface area of the powder samples was calculated from adsorption data (in the relative pressure P/P_0 range from 0.05 to 0.3, where P and P_0 are the partial and saturated pressures of adsorbate, respectively) by a multipoint Brunauer–Emmett–Teller (BET) method.

2.3. Photocatalytic activity (PCA)

The decomposition of 2.5 ppm methylene blue (MB) solution was used to evaluate the photocatalytic behaviour of the synthesised Ag/ZnO nanocomposite systems. Before each experiment, to achieve the adsorption equilibrium, 5 mg of synthesised samples were dispersed in 600 ml of MB solution in a Pyrex glass reactor and magnetically stirred for 40 min in the absence of light. Then, the photocatalytic reaction was conducted under the irradiation of a UV light lamp (125 W high-pressure mercury vapour, Jinfei Company, Shanghai) at RT with continuous stirring during 2 h.

To follow the decomposition process as a function of reaction time, during the photocatalytic process, a constant volume (an aliquot of 3 ml) of the solution was taken at different reaction times (0, 5, …, 90, 120 min). All these aliquots were kept in the dark and at low temperature (< 5 °C), in order to avoid that the photocatalytic reaction continued. The sedimentation process was used for preventing the scattering effect. After that, only the liquid was taken for evaluating the MB concentration by measuring the optical absorbance with a Lambda 14P UV–visible spectrophotometer.

3. Results and discussions

3.1. X-ray diffraction (XRD)

Fig. 1 represents the XRD patterns of Ag/ZnO systems obtained by (a) single and (b) two- steps USP, respectively. All powders exhibited the typical pattern for the hexagonal wurtzite structure of ZnO (JCPDS 89–1397). Moreover, peaks marked with '*, corresponding to metallic Ag with FCC structure were also found (38.2°, 44.4°, 64.6°, 77.6° and 81.8°) being all consistent with the reported values (JCPDS 87-0720), indicating that at 800 °C the $AgNO_3$ had fully decomposed. Besides ZnO and Ag, there is no other peak detected, suggesting that phase pure

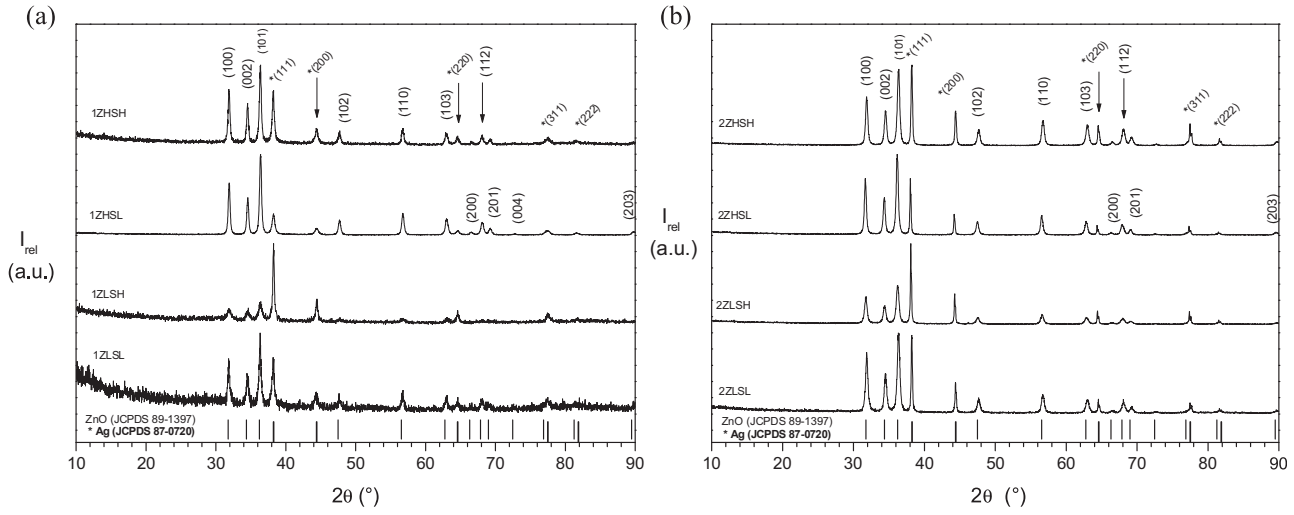

Fig. 1. XRD patterns of Ag/ZnO nanocomposite systems synthesised by (a) single step USP and (b) two − steps USP.

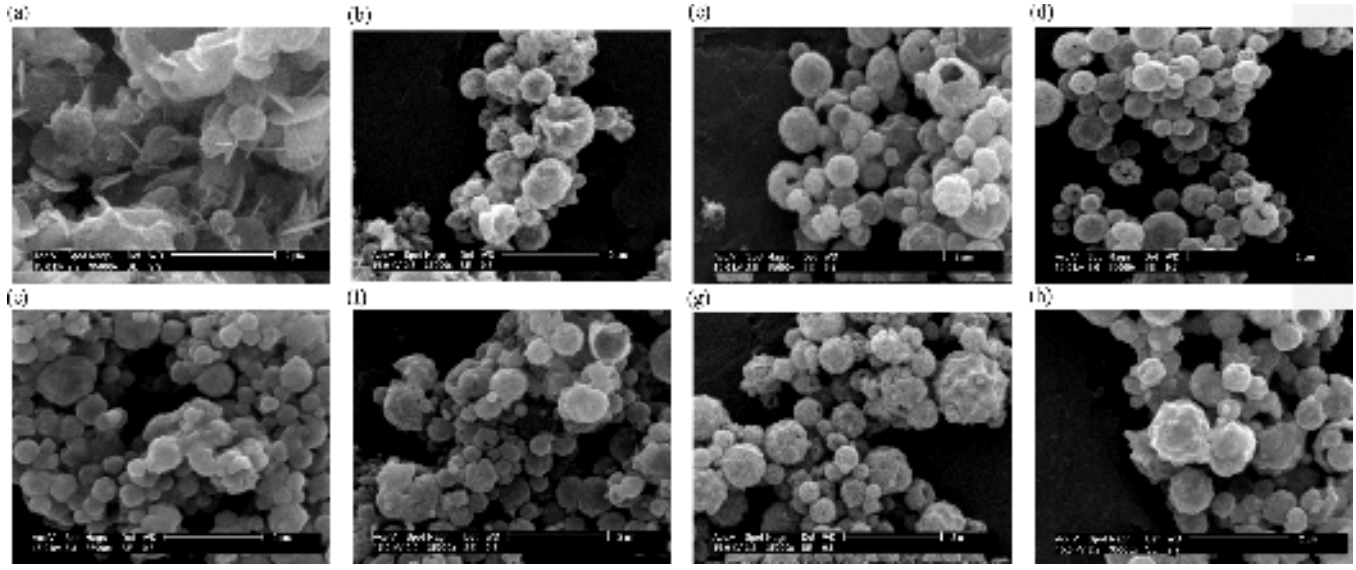

Fig. 2. Low magnification scanning electron micrographs (SEM) of Ag/ZnO systems synthesised by one and two-steps at various precursor concentrations (a) 1ZLSL, (b) 1ZLSH, (c) 1ZHSL, (d) 1ZHSH, (e) 2ZLSL, (f) 2ZLSH, (g) 2ZHSL and (h) 2ZHSH.

powders were obtained without any unreacted precursor phase or secondary phases. It is worth to emphasise that the presence of various amounts of silver did not change the corresponding peak positions of ZnO implying silver does not affect the crystal structure of ZnO. Furthermore, there was no noticeable change in the intensity ratios of the peaks. However, a slight widening and attenuation of the peaks were observed in lower zinc concentration samples synthesised via single step USP, which indicates smaller crystal size and/or low crystallinity. As expected, at highest Ag^{+}/Zn^{2+} molar ratio = 0.4 (sample 1ZLSH) a peak corresponding to silver exhibited the highest intensity and decreased proportionally with reduction of Ag content. Also, when compared with single step USP synthesis products, two steps USP products revealed sharper and well-defined peaks suggesting that the samples crystallised better, or exhibited bigger crystals.

In Table S2, the crystallite size (CS) calculated based on the FWHM of the most intense peaks, (111) for Ag and (101) for ZnO, are listed. The CS of ZnO was determined in the range of 35–42 nm and 49–69 nm for the single and two-steps USP, respectively, independent of different Ag precursor solution concentration. The relatively bigger crystallite size might be explained by diverse formation mechanisms of single, and two step derived samples. In a single step, both precursors are atomised and together, experience the nucleation and growth stages. However, in two steps, separate nucleation and growth of ZnO take place and then they meet with silver nitrate droplets which were atomised separately. Presence of Ag in a single step may result in mobility decrease of ZnO crystal boundaries and restricts their growth. Although residence time [15] is higher in one step, which expected to yield in bigger crystals, inhibitor effect of Ag on ZnO boundary is more pronounced and yield in relatively finer crystals concerning two step samples. The average crystallite size for silver was calculated to be in the range of 21–32 nm as also listed in Table S2. In a general manner, by varying reaction steps and% Ag content, there was not a dramatic change observed in Ag crystal size. However, when single − and two steps USP derived values of the same concentration samples are directly compared, it is observed that all two step samples exhibit coarser crystallite size. Nevertheless, despite finer crystallite sizes of single step samples, their XRD patterns exhibit more pronounced peak broadening when compared with two step samples. Presence of Ag during crystallisation of ZnO may result in poor crystallinity and more structural defects which also causes peak broadening [16,17]. Amorphous like XRD diffractograms of single step samples with background humps are also parallel with lack of crystallinity. Moreover, this will be investigated in details with SEM/TEM

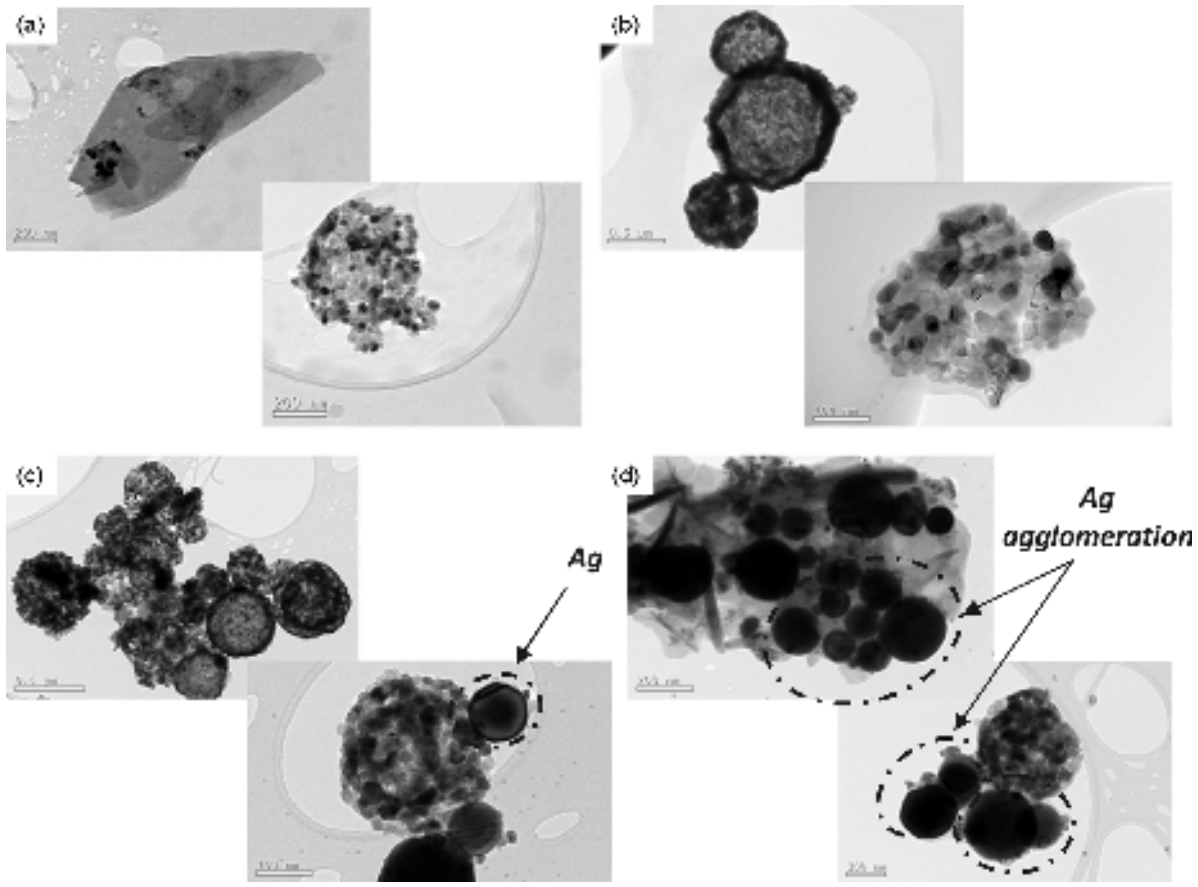

Fig. 3. High-magnified TEM micrographs of Ag/ZnO structures synthesised at various precursor concentrations: (a) 1ZLSL, (b) 1ZHSH, (c) 2ZLSL and (d) 2ZLSH.

micrographs.

3.2. Scanning electron microscopy (SEM)

Scanning electron microscopy (SEM) images of Ag/ZnO samples synthesised *via* single step USP represented in Fig. 2 reveal microstructural differences as a result of initial precursor solution concentration variation. Sample 1ZLSL, where both constituents are in lower concentration, exhibited entangled plate and desert rose-like morphology accompanied by granules. Similar morphologies have also been reported in previous studies for other methods such as; electrodeposition and hydrothermal synthesis and related to low supersaturation. Lower supersaturation decreases the driving force to nucleation take place, and Bessel-Cabrera-Frank growth model occurs liberated by screw dislocation movement and leading to rod or planar growth [18,19]. This entangled plate morphology in low initial concentration sample has been consistent with the findings of previous studies. Moreover, lower precursor concentration leads to smaller droplet size and higher fasting rates, which results in porous and exploded particles. When noisy XRD pattern with broadened peaks of 1LZLS is considered, where low crystal quality and some amorphous content is emphasised, this may be caused by fast reaction rates that deviate from equilibrium conditions. Furthermore, this difference in crystallinity may also be based on different growth mechanism lead by dislocations without nucleation. In contrast, in the case of higher silver concentration, this plate morphology was replaced with spherical like irregular granules. This indicates that the incorporation of Ag into system changes nucleation and growth behaviour of zinc phase.

Other samples consistent with previous studies exhibited roughed spherical like morphology with some defected surfaces, where an opening is visible, probably due to explosions [20]. Moreover, SEM images also revealed some hollow spheres with pores on their surface. This morphology should be caused by solvent (here, the water) evaporation characteristic time is shorter than the solute diffusion characteristic time. This may cause solute concentration gradient, which has a high influence on the particles morphology as previously reported [19]. In addition, there are studies [21] where this morphology at low temperatures ($< 300\ ^{\circ}C$) in USP method, is also related to critical supersaturation and precipitation. In the case of low zinc concentration samples, a direct comparison regarding particle size is not possible due to various leading morphologies. Even though, when Fig. 2c and d are compared, it is worth to emphasise that, as silver content increases, a decrease in particle size was observed. The reason for this change may be found insight reaction mechanism. In single step USP, a droplet including both precursors evaporates, thermal decomposition takes place, and firstly core particle reaches super saturation and precipitate. This process is followed by precipitation of shell material. The details of this process can be found in our previous research [12]. The decrease in particle size can be related to obstacle effect of silver on already precipitated ZnO surface boundary movement, and this may be an indicator of proximity to target core-shell morphology where most of Ag precipitates on the surface with minimum entrapment in volume.

In Fig. 2, SEM micrographs of two step USP Ag/ZnO products also represented with various silver and zinc concentration as identical to one-step samples. In a general manner, all samples exhibited similar spherical-like morphology. As it was expected, when the flow rate was increased (as two steps-USP), shorter residence time was obtained, which could affect particle size. There are studies [22] which demonstrate that with higher flow rate, the flowing regime is more turbulence, and therefore contact between molecules increases, raising the collision and coalescence between drops and leading more agglomeration and hence to higher particle sizes. In parallel, relatively coarser particles of

two-step synthesis were remarkable with respect to one step samples which was also revealed by BET analyses. This difference may also be related to different formation mechanisms of core shell structures via one and two step USP, inhibiting the effect of Ag on ZnO surface as explained previously. In the case of two steps USP, if the collision between ZnO and $AgNO_3$ droplets were successful this particle size decrease would also be observed; however, coarser size may also be considered as a signal of the high amount of unsuccessful collision. Moreover, agglomeration of silver nanoparticles separately or on top of ZnO core may also yield in bigger particle size. In addition, lower zinc content samples include mainly finer particles as expected regarding concentration and particle size relation [23] as shown in Fig. 2e and f. Moreover, a significant variation in particle size range in two steps samples may be an indication of separate precipitation of Ag and ZnO without a successful collision: this will be further investigated by TEM.

3.3. Transmission electron microscopy (TEM)

Transmission electron microscopy (TEM) analysis was performed on selected samples to lighten morphological features in details with a comparative manner between single and two steps USP. The micrographs of the Ag/ZnO multicomponent nanoparticles are presented in Fig. 3. The silver nanoparticles are easy to spot and differentiate from the oxide primer particles by their colour on the TEM micrograph. The silver nanoparticles are darker than the one oxides, which is the consequence of sufficient density difference between them (10.49 g/cm^3 for silver, 5.61 g/cm^3 for zinc oxide) [12].

From Fig. 3, it is easy to see that ZnO is found as secondary spherical nanoparticles, which are constructed by primary fine crystals, aggregated and/or even sintered, with a size range of 5–20 nm. Fig. 3a reveals ZnO plates accompanying spherical morphology. It can be observed that some silver nanoparticles are also present on the ZnO plate surface and dendritic growth of plate is more dominant in the silver free zone. This is consistent with SEM findings, which implies that the presence of Ag changes ZnO growth process and modifies the morphology into spheres. When the surface area to volume ratio of sphere and plates are considered, as also revealed by BET, with modification of morphology, a significant increase in surface area was achieved in 1ZLSL which may favour PCA. Fig. 3b reveals TEM micrograph of the sample with highest BET surface area among spherical single step synthesised samples. It is obviously seen that close to target morphology, thin and homogeneous Ag layer deposition on top of ZnO was achieved. When these TEM micrographs are considered together with EDX analyses provided in Table S3, it can be seen that in single step samples, increasing Ag concentration favours ZnO surface coverage. In the case of two steps USP synthesised samples, TEM micrographs revealed that morphology is not as promising as single step samples. The most propitious sample regarding target microstructure (2ZLSL) among all two steps samples is presented in Fig. 3c with relatively homogeneously and mostly on the top of ZnO surface deposited Ag nanoparticles; as well as small amount of agglomerated Ag clusters. As Ag concentration increases, separate agglomerated silver particles labelled in Fig. 3d were detected, which proves unsuccessful collision as mentioned previously in XRD and SEM parts. The variation in silver content revealed by EDX (samples 2ZLSL and 2ZLSH present wt.% 11.79 and 17.33, respectively) leads to more and bigger (around 100–200 nm) silver agglomerations which are detrimental to PCA. These findings highlight the importance of Ag concentration adjustment to obtain desired morphology. Owing to different formation mechanisms for single and two steps USP, silver concentration affects ZnO surface coverage reversely.

3.4. Growth mechanism of Ag/ZnO nanocomposites

On the one hand, the decomposition of zinc nitrate hexahydrate during spray pyrolysis takes place in several reaction steps. Previous works [24] have been proposed the mechanism of the thermal decomposition, which is formally described and balanced by us as follows:

$$Zn(NO_3)_2{\cdot}6H_2O \rightarrow Zn(NO_3)_2{\cdot}H_2O + 5H_2O\uparrow \quad (1)$$

$$3Zn(NO_3)_2{\cdot}H_2O \rightarrow Zn(NO_3)_2{\cdot}2Zn(OH)_2 + H_2O\uparrow + 4NO_x\uparrow \quad (2)$$

$$Zn(NO_3)_2{\cdot}2Zn(OH)_2 \rightarrow 3ZnO + 5H_2O\uparrow + 2NO_x\uparrow \quad (3)$$

In this process, the formation of some oxides of nitrogen through some intermediate products takes place too, such as [25]:

$$Zn(NO_3)_2 \rightarrow \rightarrow ZnO + yN_wO_x + zO_2 \quad (4)$$

However, there is a well-known agreement that the final product of all intermediate product decomposition is zinc oxide (ZnO).

On the other hand, the precipitation reaction is known to be one of the most common liquid phase reactions to form a solid phase. Also, the solubility of precursors plays a major role in supersaturation effect. Both present high solubility in cold water (184 and 222 g/100 ml water, at 20 °C, for zinc and silver nitrate, respectively). Zinc nitrate loses six water molecules at 36.4 °C and melts at 212 °C. However, the solubility of silver nitrate rises rapidly with increasing the temperature (952 g/100 ml water at 100 °C). Therefore, the different USP constructions for the synthesis (single or two steps) affect highly on precipitation step.

Hence, on the basis of previous studies and micrograph result mentioned above, a growth mechanism of the Ag/ZnO USP-nanocomposite systems has been proposed, which is shown in Fig. S2. In the single step USP, both precursors were mixed. So, the aerosol droplets contained a mixture of two nitrates (zinc −ZN- and silver −SN-), which were transferred to the furnace (at 800 °C) by the carrier gas, where the thermal decomposition and then co-precipitation took place into the defined droplet volume (spatial limitation). Since there are some differences in supersaturation concentration between zinc and silver nitrates, the core-shell particle morphology is obtained (as shown for 1ZHSH, Fig. 3b). Moreover, the heterogeneous nucleation of both components and the spatial limitation probably caused the smaller ZnO particle sizes, which should be due to the inhibiting effect of the silver particle on the growth of ZnO. In the two steps USP, in the first part, where only ZN was dissolved in the precursor solution, the aerosol was formed and then brought into a high temperature zone. ZN droplet precipitated into droplet volume, and consequently, ZnO nucleated homogeneously. In the second part, droplets containing silver nitrate were added, which met with ZnO particles already formed in the first furnace. So, two cases were possible: (i) collision among ZnO particles and SN droplets, causing silver nitrate precipitation and nucleation onto ZnO particle surface and producing a similar inhibiting effect of silver on ZnO growth (2ZLSL, Fig. 3c), or (ii) silver nitrate precipitation and then nucleation into ZnO droplet and afterwards collision among ZnO and Ag particles (ZLSH, Fig. 3d).

3.5. UV–vis diffuse reflectance spectroscopy (DRS)

The UV–vis diffuse reflectance spectra of all samples were studied. The band gap energy was measured by the extrapolation of the linear portion of the graph between the modified Kubelka −Munk function $(F(R){\cdot}h\gamma)^2$ *vs* photon energy ($h\gamma$) [13], as shown as an example in Fig. 4. The band gap values are listed in Table S2. It was found that band gap of most samples was very similar and around 3.24 eV (3.24 eV < > 383 nm). Sample 1ZLSL exhibited highest band gap value of 3.27 eV which may be due to its different plate dominated morphology and aspect ratio as also previously reported in the literature [26]. Moreover, all samples have smaller band gap value with respect to the theoretical value of 3.37 eV. This band gap narrowing phenomena is also consistent with previous reports which declare the decrease of band gap energy with donor energy levels provided by dopants or alloying elements. It is originated from the charge transfer between d-type

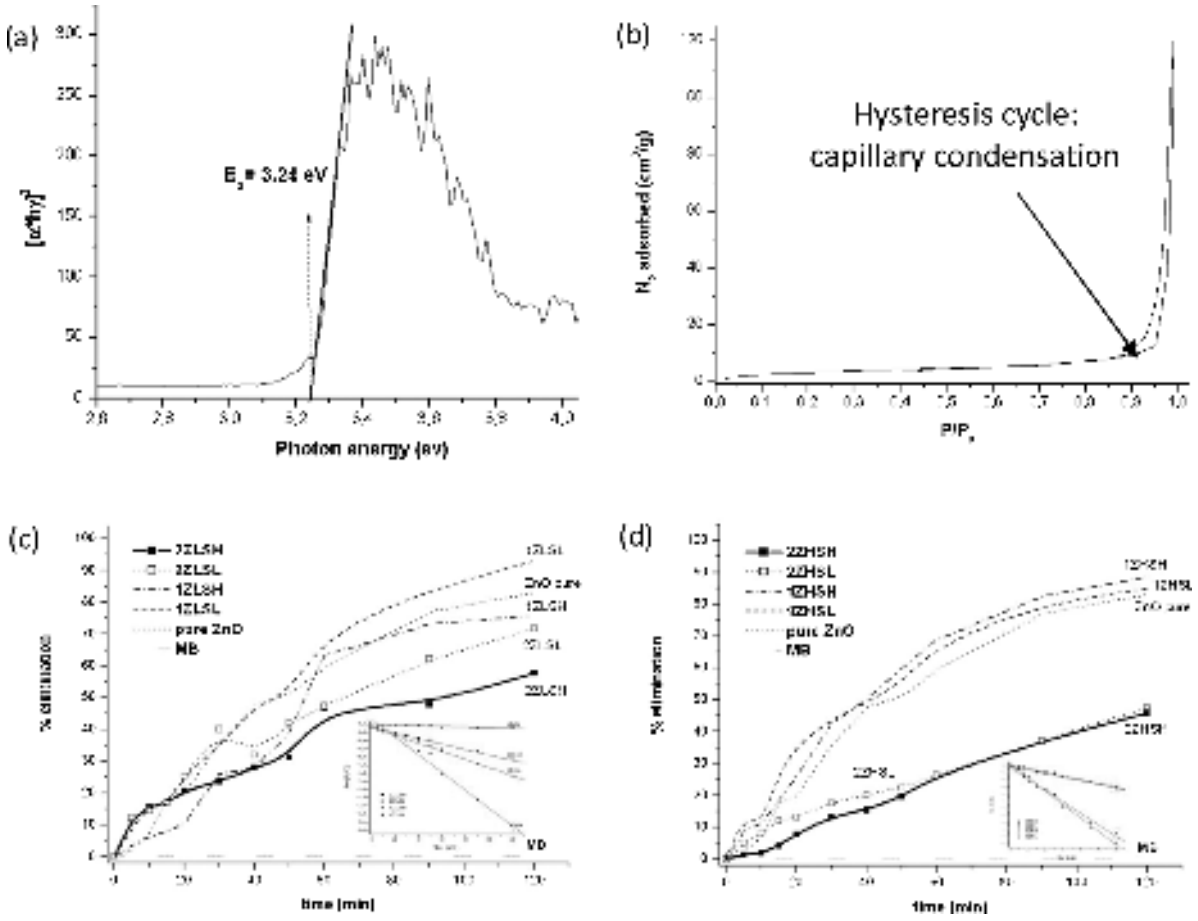

Fig. 4. Examples of (a) band gap value estimation from the Kubelka-Munk equation from UV–vis DRS and (b) the N_2 adsorption/desorption isotherms. Photocatalytic activity of Ag/ZnO systems by% elimination of methylene blue (MB) solution under UV irradiation. Systems synthesised with (c) low and (d) high zinc precursor concentration, respectively. Inset: plot of $Ln(C_t/C_0)$ versus degradation time.

electrons of Ag and conduction band of semiconductor oxide. [27,28]. Moreover, PCA of ZnO can be improved by plasmon resonance as studied by other researchers [27,28]. Oscillating surface plasmons on the surface of silver nanoparticles interact with light and improve the ZnO light absorption capability. However, when they form aggregates, they can also act as scattering and electron-hole recombination centre as mentioned before. This hypothesis agrees with our experimental results, which implies the better distribution of silver nanoparticles on the surface of ZnO yield in more enhanced photocatalytic activity. This also underlines the importance of size and distribution of Ag nanoparticles [1,29,30].

3.6. Measurement of the surface area (BET, N_2 gas adsorption/desorption)

A representative N_2 adsorption–desorption isotherm (Fig. 4) reveals that prepared Ag/ZnO nanocomposite catalysts comprised of mesopores and displayed the typical type IV curve (according to the IUPAC classification, where mesoporous solids have A_{BET} = 10–200 m^2/g y $ø_{poro} \approx 2 - 50$ nm). This curve presents a hysteresis cycle at higher relative pressures (P/P_0 = 0.85–0.99) which are associated with the filling and emptying of mesopores and the presence of micropores on the surface. The considerable rise in nitrogen adsorbed quantity at the highest relative pressures is usually related to the agglomeration phenomena [11]. The specific surface area values of all systems are listed in Table S2. The highest value was obtained for sample 1ZLSL; this can be due to the different morphology (greater surface area of plate morphology concerning spherical particles where the surface is minimised) of this sample. This value could be caused by the fact that the high temperature (800 °C) was used in both reaction zones. Therefore, ZnO particles formation took place already the first zone, and after that, the high temperature leads to ZnO particles continued to grow in the second one, which decreased the specific surface areas. As it can be seen in Table S2, BET surface areas decreased from 12.5 to 8.8 m^2/g, when the Ag^+/Zn^{2+} molar ratio of precursors increased from 0.1 to 0.4. In the case of two steps synthesis, the BET surface areas decreased further up to 6.5-2.3 m^2/g indicating that agglomeration of ZnO and Ag particles away from target core-shell characteristic particle morphology [31].

3.7. Photocatalytic activity (PCA)

The photocatalytic behaviours of the as-prepared Ag/ZnO catalysts were investigated in the degradation of methylene blue (MB) dye reaction under UV light. The catalytic performance regarding the percentage of methylene blue elimination is given in Table S2 [5]. Moreover, to determine the presence of MB absorption phenomena, the percentage of degradation of MB exposed at UV lamp without any catalysts has also been included (curve called “MB”). As it can be observed, in the absence of photocatalyst, the concentration of the MB remains almost constant implying the degradation of the pollutant does not take place. Therefore, it is possible to suggest that absorption phenomena are negligible or absent.

Among single step USP samples, at the end of 2 h, the highest degradation of MB value of 93% is achieved by sample 1ZLSL where surface area is maximised with planar morphology as different from other samples, and the Ag^+/Zn^{2+} molar ratio is 0.2. Following that, highest second value (88%) achieved by 1ZHSH same Ag^+/Zn^{2+} molar ratio of 0.2 where spherical particles are observed. When Ag^+/Zn^{2+}

molar ratio is decreased to 0.1 (1ZHSL) and increased to 0.4 (1ZLSH), PCA decreased to 85% and 76%; respectively. These findings indicate optimum loading of Ag is satisfied for the Ag^{+}/Zn^{2+} molar ratio of 0.2 and surface area is the superior dominating factor for improved PCA. The inclusion of a low loading of Ag on ZnO particles surface allows that the silver acts as trap photo-induced electrons, retarding the electron–hole recombination process, and thereby, promoting the PCA. However, there are studies where it has been observed that when there was an excessive amount of ion metal (M^{n+}) on the catalyst surface, a larger amount of M^{0} species could be produced, resulting in an alloy formation or solution–solid, and as a consequence the catalyst activity decreases as observed on sample 1ZLSH [32]. In the two steps USP synthesised catalysts, this effect is also similar. On the other hand, it can be seen that the systems prepared by different techniques (similar precursor content), one step USP catalysts was found to have much more activity than the others (two steps ones), suggesting the possibility for blockages of the active surface of ZnO due to higher particle sizes. Fig. 4 shows the MB degradation as a function of time using Ag/ZnO catalyst under UV irradiation. Comparing the different experimental conditions, following trend of the PCA and SSA can be observed: 1ZLSL > 1ZHSH > 1ZHSL > 1ZLSH > 2ZLSL > 2ZLSL > 2 ZHSL > 2ZHSH. This result proves the importance of the specific surface area for high PCA. Beyond SSA, particularly, the effect of Ag addition was evaluated. In Fig. 4c and, it can be seen that PCA curve for ZnO is also provided for direct comparison purposes. It can be observed that all two steps synthesised Ag/ZnO samples exhibited poorer PCA concerning pure ZnO (82% of elimination). In contrast, most of the single step samples showed enhanced PCA when were compared with pure ZnO. The pollutant conversion was gradually increased during 120 min time, archiving until 93% of elimination at a single step, low Zn content leading planar morphology and intermediate (0.2) Ag^{+}/Zn^{2+} molar ratio (the best conditions). The only sample that Ag addition decreases PCA is the one with highest Ag/Zn ratio with 0.4, implying higher Ag loading.

There are two linked effects dominating the PCA: (i) surface catalytic effects and (ii) photo phenomena: the interaction of light with the material to form electron–hole pairs [33]. The first parameter is dominated by the specific surface area; whereas second improves with increasing crystal quality and also the addition of metallic nanoparticles like Ag. The results presented in Table S2 and Fig. 4 can be discussed thank to these two-effects.

The former is the available surface area which is related, among others things, with sample particle sizes. In our previous researches [4,5] it has been detected that smaller particle sizes lead to a larger specific surface area, and therefore enhance PCA because pollutant-adsorption and light-harvesting are assisted. Therefore, as it can be expected, sample 1ZLSL exhibited the best PCA owing to its high surface area of 21.8 g/m^2. Furthermore, several studies [36,34,35] have demonstrated that the ultra-thin sheet-like structures, similar to sample 1ZLSL, could enhance the efficiency of the electron–hole separation. This process, which takes place from the inside to the surface of the crystal (where they react with the organic molecules), is benefited in samples with ultra-thin thickness.

The latter is related to the higher proportion of (002) plane, which could be observed comparing samples with low and high Ag concentration, respectively (Fig. 1). According to Lu et al. [36], in this plane, the oxygen molecules and hydroxyl groups (OH^{-}) adsorption are enhanced due to its unsaturated oxygen coordination and positive charge, which could also significantly improve the PCA. Moreover, it is known that metallic nanoparticles like Ag have surface plasmons enhancing the photocatalytic activity by creating a local electric field and the optical vibration and trapping photogenerated electrons that prevent e-h recombination process. However, for these enhancements, the size and distribution of Ag nanoparticles are very critical. When they are big and agglomerated nanoparticles they can act as recombination centre [27,28] also they may inhibit contact of the solution with ZnO [37]. Findings of PCA are consistent with this knowledge and underline the importance of optimum Ag loading and distribution. Comparing particle sizes between samples 1ZHSH and 2ZLSL provided in Fig. 3b and c, it can be observed that despite it is bigger particle size, the first one leads to higher PCA. It is because sample 1ZHSH presents better silver particles distribution over ZnO surface. Moreover, relatively poor PCA of 1ZLSH and all two steps samples can be explained by isolated and agglomerated silver particles which reduce the available surface, increase the e-hole recombination and, so worsen the photocatalytic behaviour.

To determine which law describes the photocatalytic activity of these materials, the inset image in Fig. 4c and d have been included. These figures show the plotted data of $Ln(C_t/C_0)$ versus degradation time, where C_t and C_0 correspond to the concentration of aqueous MB at each reaction time ("t") and the initial one, respectively. Since this plot corresponds to a linear fit, this degradation reaction may be modelled as a pseudo-first-order reaction.

4. Conclusions

Spherical, core-shell like Ag/ZnO nanocomposites have been successfully synthesised by straightforward and economical single and two steps USP technique. Structural characterisation revealed that all samples exhibited phase mixture of FCC Ag and a hexagonal wurtzite ZnO. Mostly, all samples revealed typical USP spherical particle morphology, where Ag nanoparticles are dispersed over ZnO secondary spherical assemblage representing an agglomerate of small primary crystals in nanometric range. The different formation mechanisms with varying amounts of Ag and ZnO and two different USP installations are proposed. It was reported that with the novel two-steps USP, Ag particles exhibited the tendency to form bigger agglomerates rather than uniform and fine deposits on the ZnO surface. Therefore, they exhibited poorer PCA concerning one step samples. However, environmental applications of all synthesised samples are promising to owe to pollutant removal values higher than 45%. The best dye elimination of 93% was achieved by sample where surface area is maximised and for optimum Ag^{+}/Zn^{2+} = 0.2 molar ratio, revealing the importance of surface area and adjustment of the silver amount. Especially, the single step USP synthesis with optimum Ag loading improves the photocatalytic performance significantly and implies that USP method is highly promising in nanocomposite processing with enhanced PCA.

Acknowledgments

We gratefully acknowledge the financial support of the Autonomous Region Program of Madrid, MULTIMATCHALLENGE (ref. S2013/MIT-2862) and the "Álvaro Alonso Barba" Technological Institute of Chemistry and Materials (of Carlos III University of Madrid) sponsoring this international collaboration. We thank our colleague Peter Majerič (University of Maribor, Slovenia) who provided insight and expertise that greatly assisted the research. Authors would also like to show our gratitude to the Dr. Srećko Stopić, IME- RWTH Aachen) for sharing his pearls of wisdom with us during this research. O.M. acknowledges the financial support from the Ministry of Education, Science and Technological Development, Republic of Serbia (Projects OI172035 (1612046) and III 45020).

Appendix A. Supplementary data

Supplementary data associated with this article can be found, in the online version, at https://doi.org/10.1016/j.cattod.2017.11.029.

References

[1] H. Liu, F. Nosheen, X. Wang, Chem. Soc. Rev. 44 (2015) 3056.
[2] G. Li, Z. Tang, Nanoscale 6 (2014) 3995.

[3] R.G. Chaudhuri, S. Paria, Chem. Rev. 112 (2011) 2373.
[4] L. Muñoz-Fernandez, A. Sierra-Fernandez, O. Miloševic, M.E. Rabanal, Adv. Powder Technol. 27 (2016) 983.
[5] L. Muñoz-Fernandez, A. Sierra-Fernandez, G. Flores-Carrasco, O. Milošević, M.E. Rabanal, Adv. Powder Technol. 28 (2016) 83.
[6] Y. Zheng, L. Zheng, Y. Zhan, X. Lin, Q. Zheng, K. Wei, Inorg. Chem. 46 (2007) 6980.
[7] Y. Zheng, C. Chen, Y. Zhan, X. Lin, Q. Zheng, K. Wei, J. Zhu, J. Phys. Chem. C 112 (2008) 10773.
[8] A. Di Mauro, M. Zimbone, M. Scuderi, G. Nicotra, M.E. Fragalà, G. Impellizzeri, Nanoscale Research Letters 10 (484) (2015) 1.
[9] M.E. Fragalà, A. Di Mauro, D.A. Cristaldi, M. Cantarella, G. Impellizzeri, V. Privitera, J. Photochem. Photobiol. A: Chem. 332 (2017) 497.
[10] Y. Zhang, J. Mu, J. Colloid Interface Sci. 309 (2007) 478.
[11] X.M. Wang, Z.W. Fan, K. Zhou, Mat. Tian, Sci. Eng. B 176 (2011) 978.
[12] J. Bogovic, R. Rudolf, B. Friedrich, JOM 68 (2016) 330.
[13] U.P.A. Escobedo Morales, E. Sanchez Mora, A. Morales, E. Mora, U. Pal, Rev. Mex. Fis. S. 53 (2007) 18.
[14] F. Yakuphanoglu, J. Alloys Compd. 507 (2010) 184.
[15] T.T. Kodas, M.J. Hampden-Smith, Aerosol Processing of Materials, Wiley-Vch, 1999.
[16] L. Xu, Y.L. Hu, C. Pelligra, C.H. Chen, L. Jin, H. Huang, S. Sithambaram, M. Aindow, R. Joesten, S.L. Suib, Chem. Mater. 21 (2009) 2875.
[17] C. Wang, E. Shen, E. Wang, L. Gao, Z. Kang, C. Tian, Y. Lan, C. Zhang, Mater. Lett. 59 (2005) 2867.
[18] B.N. Illy, B. Ingham, M.P. Ryan, Crystal Growth Design 10 (2010) 1189.
[19] D. Lincot, MRS Bull. 35 (2010) 778.
[20] K.C. Hsiao, S.C. Liao, Y.J. Chen, Mater. Sci. Eng.: A 447 (2007) 71.
[21] L. Mädler, S.E. Pratsinis, J. Am. Ceramic Soc. 85 (2002) 1713.
[22] B. Honarvar, S.A. Sajadian, M. Khorram, A. Samimi, Braz. J. Chem. Eng. 30 (2013) 159.
[23] C.K. Pinyali, A.D. Rockstraw, S. Deng, Aerosol Sci. & Tech. 39 (2005) 1010.
[24] D. Hidayat, T., Ogi, F., Iskandar, K. Okuyama, 151 (2008), p. 231.
[25] S.A. Studenikin, N. Golego, M. Cocivera, J. Appl. Phys. 83 (1998) 2104.
[26] X. Zhang, J. Qin, Y. Xue, P. Yu, B. Zhang, L. Wang, R. Liu, Sci. Rep. 4 (2014) 4596.
[27] H. Lu, S. Wang, L. Zhao, J. Li, B. Donga, Z. Xu, J. Mater. Chem. 21 (2011) 4228.
[28] A.A. Mosquera, J.M. Albella, V. Navarro, D. Bhattacharyya, J.L. Endrino, Sci. Rep. 6 (2016) 1.
[29] R. Georgekutty, M.K. Seery, S.C. Pillai, J. Phys. Chem. C. 112 (2008) 13563.
[30] N. Kamarulzaman, M.F. Kasim, R. Rusdi, Nanoscale Res. Lett. 10 (2015) 346.
[31] O. Mekasuwandumrong, P. Pawinrat, P. Praserthdam, J. Panpranot, Chem. Eng. J. 164 (2010) 77.
[32] S. Pisduangdaw, J. Panpranot, C. Methastidsook, C. Chaisuk, K. Faungnawakij, P. Praserthdam, O. Mekasuwandumrong, Appl. Catal. A: Gen. 370 (2009) 1.
[33] M.J. Height, S.E. Pratsinis, O. Mekasuwandumrong, P. Praserthdam, Appl. Catal. B: Environ. 63 (2006) 305.
[34] X.C. Wang, J.C. Yu, C.M. Ho, Y.D. Hou, X.Z. Fu, Langmuir 21 (2005) 2552.
[35] L.Z. Zhang, J.C. Yu, Chem. Commun. 16 (2003) 2078.
[36] H. Lu, S. Wang, L. Zhao, J. Li, B. Donga, Z. Xu, J. Mater. Chem. 21 (2011) 4228.
[37] V. Scuderi, G. Impellizzeri, L. Romano, M. Scuderi, M.V. Brundo, K. Bergum, M. Zimbone, R. Sanz, M.A. Buccheri, F. Simone, G. Nicotra, B.G. Svensson, M.G. Grimaldi, V. Privitera, Nanoscale 6 (2014) p. 11189.